

RESEARCH ARTICLE

Imaging of viral neuroinvasion in the zebrafish reveals that Sindbis and chikungunya viruses favour different entry routes

Gabriella Passoni^{1,2}, Christelle Langevin¹, Nuno Palha^{2,*}, Bryan C. Mounce³, Valérie Briolat², Pierre Affaticati⁴, Elodie De Job⁴, Jean-Stéphane Joly⁴, Marco Vignuzzi³, Maria-Carla Saleh⁵, Philippe Herbomel², Pierre Boudinot¹ and Jean-Pierre Levrud^{2,‡}

ABSTRACT

Alphaviruses, such as chikungunya virus (CHIKV) and Sindbis virus (SINV), are vector-borne pathogens that cause acute illnesses in humans and are sometimes associated with neuropathies, especially in infants and elderly patients. Little is known about their mechanism of entry into the central nervous system (CNS), even for SINV, which has been used extensively as a model for viral encephalopathies. We previously established a CHIKV infection model in the optically transparent zebrafish larva; here we describe a new SINV infection model in this host. We imaged *in vivo* the onset and progression of the infection caused by intravenous SINV inoculation. Similar to that described for CHIKV, infection in the periphery was detected early and was transient, whereas CNS infection started at later time points and was persistent or progressive. We then tested the possible mechanisms of neuroinvasion by CHIKV and SINV. Neither virus relied on macrophage-mediated transport to access the CNS. CHIKV, but not SINV, always infects endothelial cells of the brain vasculature. By contrast, axonal transport was much more efficient with SINV than CHIKV, both from the periphery to the CNS and between neural tissues. Thus, the preferred mechanisms of neuroinvasion by these two related viruses are distinct, providing a powerful imaging-friendly system to compare mechanisms and prevention methods of encephalopathies.

KEY WORDS: Alphavirus, Chikungunya, Central nervous system, Zebrafish, Viral encephalitis, Live imaging

INTRODUCTION

The outcome of an infection depends crucially on the organs reached by the invasive pathogen, which entails a precarious balance between the pathogen dissemination strategy and host

defenses. The central nervous system (CNS) is especially vulnerable, being highly susceptible both to virus-induced cytopathic effects and to the inflammatory response itself (Swanson and McGavern, 2015). The CNS is, however, protected by specialized barriers, notably the blood–brain barrier (BBB). Neuroinvasion is generally rare, but some viruses have evolved strategies to enter and spread within the CNS. These mechanisms have been characterized using a variety of approaches (reviewed by Koyuncu et al., 2013), and fall within three categories. Some viruses are able to infect cells of the BBB (i.e. endothelial cells that form brain microvessels) or other components of the brain–periphery interface, such as epithelial cells of choroid plexuses. This allows their release in the brain parenchyma by the infected cells and/or disruption of the barrier causing leakage of blood-borne virions. Another strategy is known as the ‘Trojan horse’ entry, whereby viruses hide in monocytes or macrophages, and exploit the ability of these cells to cross the barrier to enter the brain. Finally, various viruses travel within the numerous axons of motor or sensory neurons that connect the CNS to the periphery, using either anterograde or retrograde transport.

Persistent or ‘stable’ infection of the CNS is a rare occurrence, except for some specialized viruses. On the contrary, acute CNS infections are often caused by zoonotic pathogens, for which humans normally represent a ‘dead-end host’ (Gubler, 2001). In particular, among the arboviruses (viruses transmitted by arthropod vectors), Alphaviruses constitute a major source of viral zoonotic diseases, and often induce encephalitis. Among Alphaviruses, Eastern (EEEV) and Western Equine Encephalitis viruses (WEEV) (Paessler and Taylor, 2011) and the re-emerging chikungunya virus (CHIKV) have been associated with serious neurological manifestations (Economopoulou et al., 2009). Sindbis virus, the type species and best-studied member of the *Alphavirus* genus, has been extensively used as a viral encephalitis model in mice (Lewis et al., 1996; Lustig et al., 1988).

Despite their importance as encephalitogenic pathogens, the mechanisms of entry of Alphaviruses in the CNS are poorly understood. SINV is well known to infect neurons and has been used as a tool to trace neural circuits (Furuta et al., 2001); however, in most experimental settings it is inoculated directly in the CNS. SINV can enter the CNS from the periphery, especially in newborn mice, but this route of entry has not been the subject of detailed investigation. Experiments in mice with a luciferase reporter virus inoculated in the footpad were consistent with an entry via peripheral nerves (Cook and Griffin, 2003), but alternative entry routes were not ruled out. In the case of CHIKV, human infants infected with the virus often display signs of encephalitis (Arpino et al., 2009; Das et al., 2010). However, a murine model showed that after peripheral injection, CHIKV-infected cells were found in the meninges but not the brain parenchyma (Couderc et al., 2008).

¹Virology and Molecular Immunology, INRA, Université Paris-Saclay, Domaine de Vilvert, Jouy-en-Josas F-78352, France. ²Macrophages and Development of Immunity, Institut Pasteur, CNRS UMR 3738, 25 rue du docteur Roux, Paris F-75015, France. ³Viral Populations and Pathogenesis Unit, Institut Pasteur, CNRS UMR 3569, Paris F-75015, France. ⁴Tefor Core Facility, Paris-Saclay Institute of Neuroscience, CNRS, Université Paris-Saclay, Gif-sur-Yvette F-91190, France. ⁵Viruses and RNA Interference, Institut Pasteur, CNRS UMR 3569, Paris F-75015, France.

*Present address: Institut de Recherches Servier, Croissy-sur-Seine F-78290, France.

‡Author for correspondence (jean-pierre.levrud@pasteur.fr)

 J.-P.L., 0000-0001-6775-2416

This is an Open Access article distributed under the terms of the Creative Commons Attribution License (<http://creativecommons.org/licenses/by/3.0>), which permits unrestricted use, distribution and reproduction in any medium provided that the original work is properly attributed.

If inoculated intranasally, CHIKV could be found in neurons from the olfactory bulb (Powers and Logue, 2007), but no further spread was documented.

A major hindrance in detailed kinetic analyses of CNS viral invasion lies with the difficulty in observing these events in real time. Despite the development of virus mutants built to express reporter genes [e.g. luciferase, green fluorescent protein (GFP), mCherry], intravital imaging of virus infection in mammals is still a real challenge (Rameix-Welti et al., 2014). The zebrafish larva offers a powerful system to follow such events in a vertebrate, being small, transparent and tolerant of prolonged anaesthesia (Levrud et al., 2014). In a recent study, we performed real-time imaging of zebrafish larvae inoculated with a GFP recombinant CHIKV (Palha et al., 2013). The majority of infected cells were found in various peripheral organs; however, infection of some brain cells, which survived much longer than cells infected in the periphery, always occurred. This work demonstrated that it is possible to image neuroinvasion in zebrafish larvae from the earliest stages of the infection. In order to gain a better understanding of *Alphavirus* neuroinvasiveness, we decided to analyse the entry route of CHIKV into the CNS in zebrafish and to compare it with a SINV infection model, thus taking advantage of the extensive knowledge available for this virus. Indeed, non-replicative SINV has been successfully used to label zebrafish neurons *in vivo* (Zhu et al., 2009); moreover, we recently showed that intracranial inoculation of zebrafish larvae with a replicative SINV strain leads to extensive and progressive brain infection (Mounce et al., 2016).

Here, we first show that upon intravenous (IV) inoculation in zebrafish larvae, SINV infects multiple cell types and replicates efficiently. Moreover, in half of the infected larvae the virus reaches the CNS, where its progressive spread can be documented by *in vivo* imaging. We tested the different possible routes of invasion of the

CNS for CHIKV and SINV. We looked at infection of endothelial cells of the BBB using high-resolution, whole-brain confocal imaging. Some CHIKV-infected cells were systematically found in co-localization with the brain vascular endothelium. Conversely, SINV did not infect endothelial cells or cause leakage of the BBB. We excluded macrophage-mediated entry as a significant mechanism for either virus. Macrophages were not productively infected, and their depletion did not prevent or delay CNS invasion. Time series of trunk infection suggest strongly that SINV can be transmitted from infected muscle fibres to their innervating spinal cord neurons; no such event occurred with CHIKV. To test whether axonal transport favoured viral spread, we injected the viruses in the retina, which revealed efficient invasion of connected brain regions with SINV, but much less so for CHIKV.

Thus, we developed zebrafish models of infection to study viral entry in the CNS using high-resolution intravital imaging approaches. Our study reveals the conservation of neurotropism of Alphaviruses from mammals to fish based on distinct entry routes in the CNS, namely infection of endothelial cells of the BBB for CHIKV in contrast to axonal transport from peripheral nerves for SINV.

RESULTS

Course of SINV infection after peripheral inoculation

Wild-type (WT) zebrafish larvae were inoculated IV at 3 days post-fertilization (dpf) (Fig. 1A) with $\sim 10^2$ plaque forming units (PFU) of SINV-GFP, similar to the protocol used for CHIKV-GFP (Palha et al., 2013). Both viruses have been engineered to induce GFP expression in infected cells under the control of an additional subgenomic promoter, reflecting expression of viral structural genes (Hahn et al., 1992; Tsetsarkin et al., 2006), and will hereafter be referred to as SINV and CHIKV, respectively.

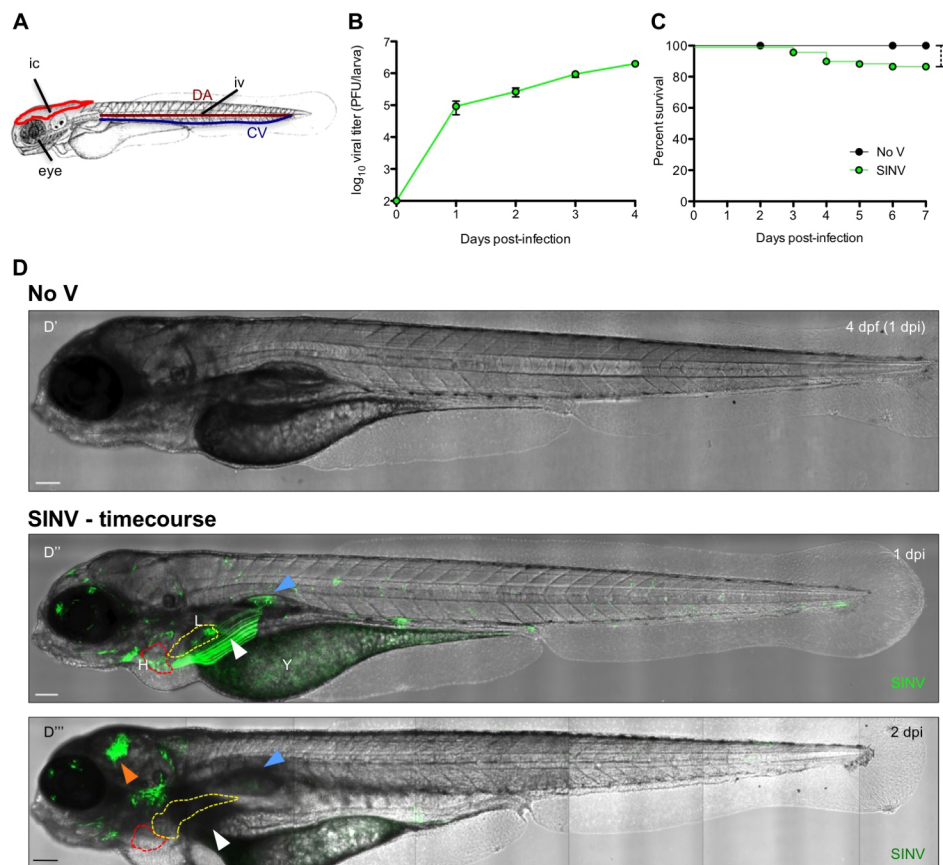


Fig. 1. SINV replicates in zebrafish larvae and exhibits a broad organ tropism.

(A) Scheme of a 72 hours post-fertilization (hpf) larva, showing the sites of injection: IV, intravenously in the caudal vein (CV) or the dorsal aorta (DA); IC, intracerebrally in the optic tectum; eye, in the retina. (B) Virus replication in IV-infected zebrafish larvae, assessed by titration of homogenates of whole larvae. Data represent the means \pm s.e.m. of five individual larvae per time point, from three experiments pooled. (C) Survival curves of control uninfected (No V) and IV-infected zebrafish larvae (SINV). Data were pooled from five independent experiments. $n=60$ larvae per group. (D) Live detection of SINV-infected cells by *in vivo* confocal imaging, with superposition of transmitted light and GFP fluorescence (maximal projection). (D') Uninfected control (No V), 4 dpf (1 dpi). (D'', D''') The same IV SINV-infected (SINV) larva at 1 dpi (D'') and 2 dpi (D'''). H, heart (dotted red line); L, liver (dotted yellow line); Y, yolk (note that the yolk is autofluorescent but, as shown in D', at a nearly undetectable level using these imaging conditions; the signal in D'' corresponds to infection); white arrowhead, infection in the left pectoral muscle; blue arrowhead, infection in the swim bladder; orange arrowhead, infection in the brain. Scale bars: 50 μ m. In this and all following lateral view figures, anterior is to the left and dorsal to the top.

Robust SINV replication was demonstrated by titrations from homogenates of larvae at different times post-injection (Fig. 1B). However, mortality was limited (Fig. 1C). Observation of SINV-infected larvae with a dissecting stereomicroscope showed that relatively mild and usually transient signs of disease appeared as early as 2 days post-injection (dpi), including oedema, irregular heartbeat and yolk opacification. In a minority of larvae (~15%), these signs persisted and led to death at ~4 dpi. The other larvae appeared to recover; however, we did not assess long-term persistence of the virus in order to avoid the additional variability entailed by feeding the larvae. Live fluorescence microscopy revealed the presence of GFP-positive (GFP⁺) cells scattered or in clusters. These infected cells were mostly observed in peripheral organs, including the liver, the heart, the yolk and in muscle fibres (Fig. 1D). Similar to what had been observed with CHIKV, infection of peripheral cells was largely transient (compare

Fig. 1Dii,Diii). These results confirm that SINV replicates efficiently in zebrafish larvae and that its dispersal through the whole organism can be monitored over time via *in vivo* imaging.

Establishment of SINV infection in the CNS

In addition, the infection often reached the CNS (brain, spinal cord, or both). Approximately half of the larvae had obvious CNS infection by 3 dpi. To assess the kinetics and frequency of CNS infection under the fluorescence microscope reliably, we used *elavl3:Gal4/5xUAS:RFP* double-transgenic larvae (hereafter called *huC:G/U:RFP*), in which red fluorescent protein (RFP) is expressed in postmitotic neurons, thus clearly delineating CNS boundaries. The kinetics and frequency of appearance of infected cells was established by repeated observation of live infected larvae. The first infected cells to appear after IV injection, observed ~8 h post-infection (hpi), were in the periphery (e.g. muscle cells, cells in the

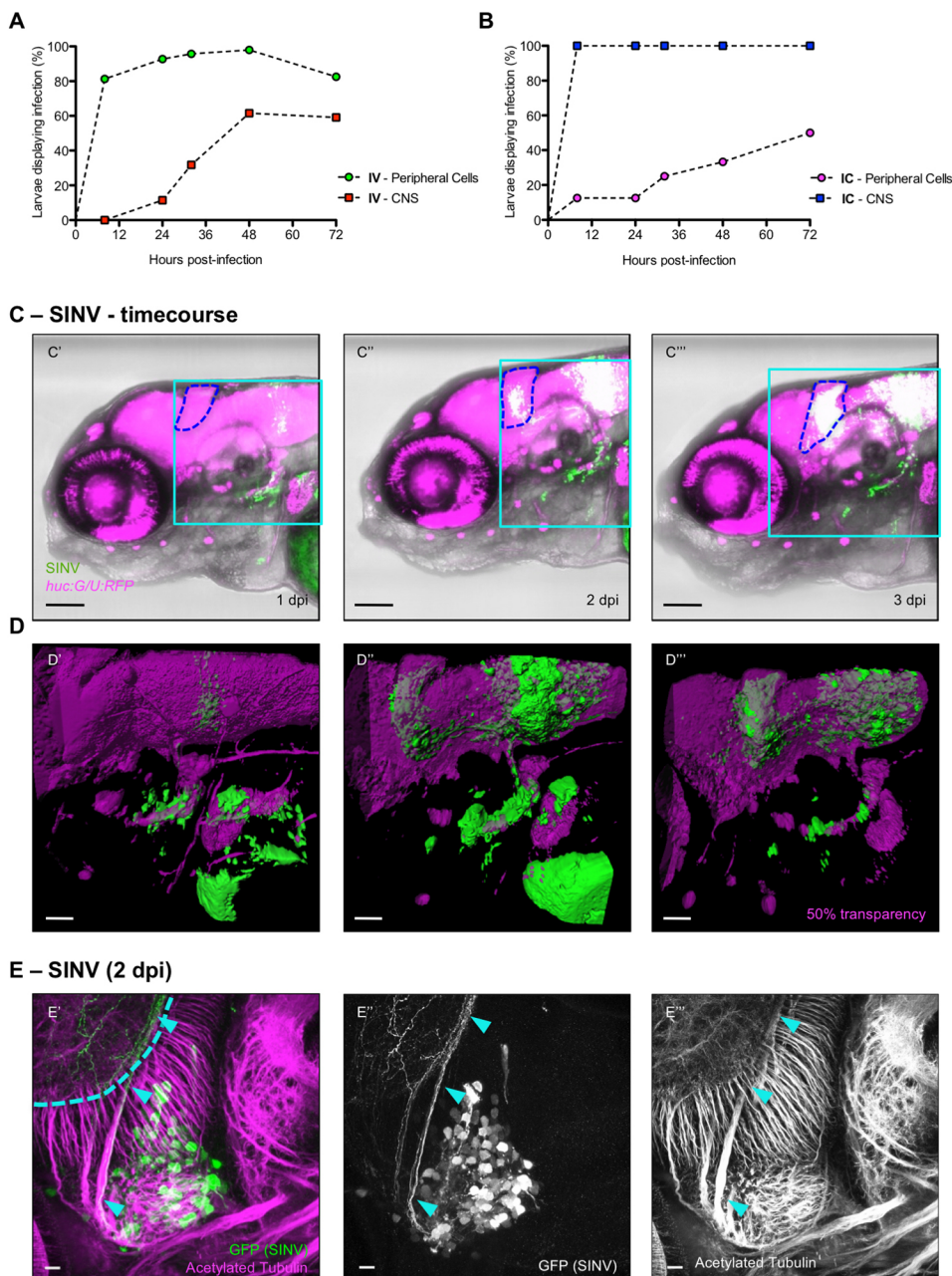


Fig. 2. SINV is neuroinvasive in zebrafish larvae.

(A,B) Quantification of the appearance of infected cells in the periphery (circles) and in the CNS (squares), from *in vivo* observation of *huC:G/U:RFP* larvae, following IV (A) or IC (B) inoculation. $n=12-24$ from two independent experiments pooled. (C'-C''') Live confocal imaging of the same IV SINV-infected *huC:G/U:RFP* larva from 1 to 3 dpi, showing the progression of the infection. Superposition of transmitted light, green (infected cells) and red (neurons) fluorescence; blue dotted line, cerebellum. In this and following colour figures, red fluorescence is displayed in magenta and referred to as 'magenta fluorescence'. The light blue squares correspond to regions shown in panels D'-D'''. Scale bars: 50 μ m. (D'-D''') 3D rendering of the brain areas shown above. Scale bars: 25 μ m. (E'-E''') Confocal image of a whole-mount immunohistochemistry processed SINV-infected WT larva, maximal projection. GFP staining (SINV-infected cells) in green; acetylated tubulin (axons) in magenta. Infected cells are in the trigeminal ganglion (TG); the axon-rich region visible behind (light blue dotted line) is the neuropile of the left optic tectum (OT). Light blue arrowheads point to the axon of an infected neuron connecting the TG to the OT. Scale bars: 10 μ m.

heart and in the liver), followed at later time points by neurons of the peripheral and the central nervous system (between 24 and 48 hpi; Fig. 2A). We could not identify any obvious pattern in these early CNS infections, which were detected in several regions of the brain (notably the telencephalon, the optic tectum, the vestibulolateralis lobe of the corpus cerebelli and the medulla) and in the spinal cord. To exclude the possibility that neurons might take longer to express GFP once infected, we performed intracranial (IC) inoculations (Fig. 1A). In that case, GFP⁺ neurons were detected as soon as 8 hpi (Fig. 2B), indicating that late appearance of CNS infection in IV-injected larvae results from the delay of virus spreading from the periphery to the CNS.

The evolution of the distribution of infected cells was evaluated by following individual larvae every 24 h with confocal imaging. Unlike foci of infection in the periphery, which generally started to decline after 2 dpi, those observed in the brain were either persistent or progressively increasing over time (Fig. 2C). Progression of

infections was attributable both to growth of established foci (such as the one seen in the cerebellum in Fig. 2C'-C''') and to spread to other neural structures (e.g. the optic tectum in Fig. 2C'',C'''). Three-dimensional (3D) rendering of the whole-brain images (Fig. 2D) strongly suggest infection of neuronal tracts connecting newly infected structures with early ones; indeed, the connection suggested by Fig. 2C,D is consistent with established wiring of the zebrafish cerebellum (Heap et al., 2013). Co-immunolabelling of SINV-positive cells and axonal projections in WT animals confirmed that neurons were infected (Fig. 2E).

For better assessment of the persistence of the infection, we followed SINV-infected larvae up to 7 dpi. Of those larvae with patent CNS infection at 3 dpi, 92% still had detectable infection by 7 dpi (11/12, excluding those that died in the interval; three independent experiments pooled).

Thus, after inoculation of SINV in the bloodstream, peripheral cells are infected first, followed by invasion of the CNS in about half

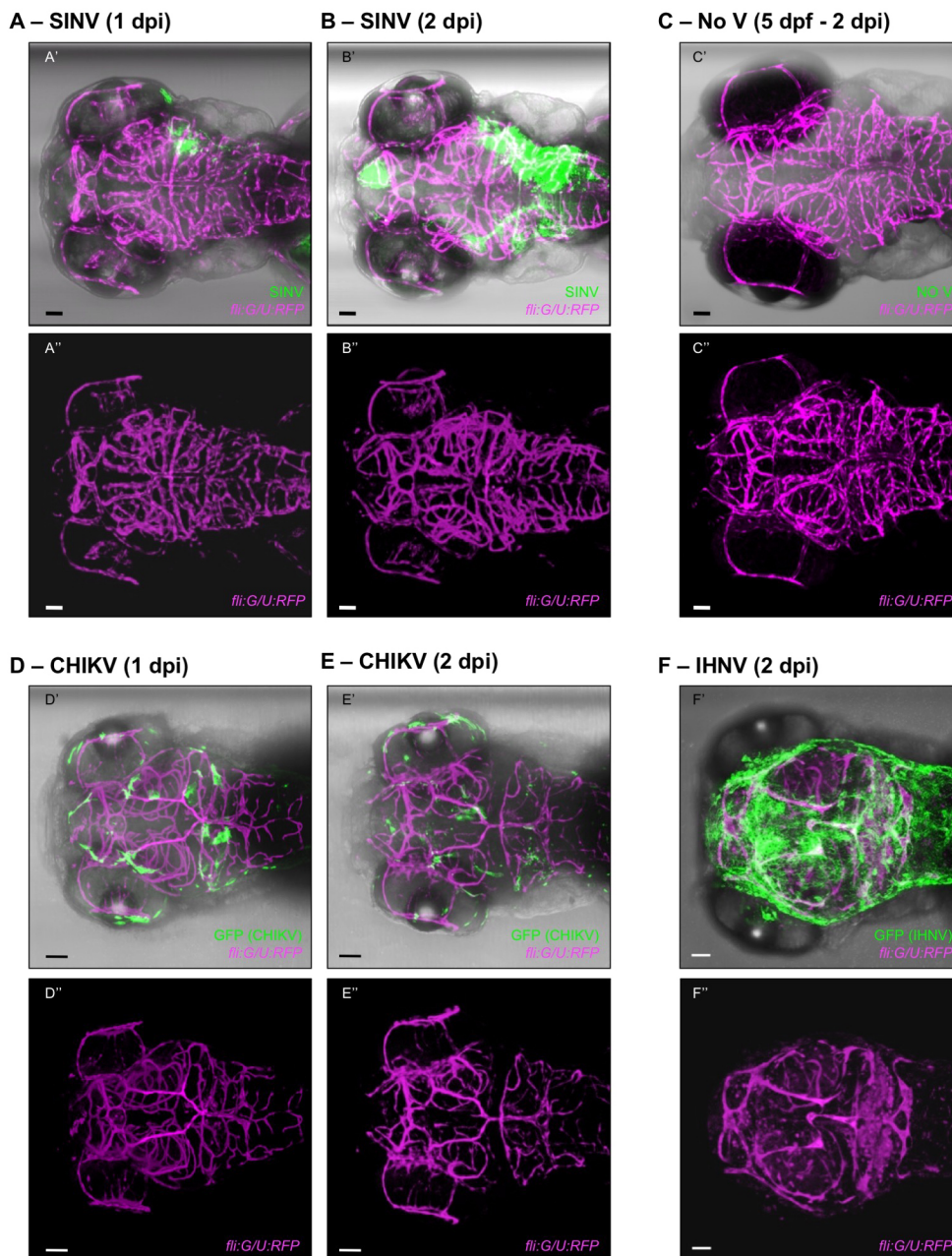


Fig. 3. CHIKV, but not SINV, infects the brain microvascular endothelium.

Dorsal views of *fli:G/U:RFP* larvae, with infected cells in green and endothelial cells shown in magenta; confocal imaging, maximal projections. For all panels, the top image (with ') shows superposition of transmitted light with green and magenta fluorescence, and the bottom image (with '') shows only the magenta fluorescence to provide better visualization of the vasculature. Scale bars: 50 μ m. (A,B) Live imaging of the same SINV-infected larva at 1 dpi (A) and 2 dpi (B). See also Fig. S1A, Movies 1 and 2, for a view through the z-stack. (C) Live imaging of control uninfected (No V) larva. (D,E) Fixed CHIKV-infected larvae at 1 dpi (D) and 2 dpi (E). See also Fig. S1B and Movie 4, for a view through the z-stack. (F) Fixed IHNV-infected larva at 2 dpi. See also Movie 5, for a view through the z-stack. In this and all following dorsal view figures, anterior is to the left.

the larvae. Peripheral infection is transient, whereas CNS infection is persistent and often spreads to other CNS structures, possibly along axon tracts.

Interestingly, the dynamics of CHIKV infection described previously (Palha et al., 2013) were fairly similar to those observed for SINV. However, CHIKV invasion of the CNS occurred in all larvae, without showing the same tendency to spread to other brain structures.

CHIKV, but not SINV, infects endothelial cells of the BBB

We then proceeded to test the possible mechanism of SINV and CHIKV entry into the CNS. A number of DNA and RNA viruses have been shown to gain access to the brain through infection of endothelial cells of the BBB, including Epstein–Barr virus (Casiraghi et al., 2011), Hepatitis C virus (Fletcher et al., 2012) and West Nile virus (Xu et al., 2012). Moreover, researchers in our laboratory previously established a zebrafish infection model of a fish rhabdovirus, infectious haematopoietic necrosis virus (IHNV), and demonstrated that IHNV primarily infects endothelial cells of the vasculature. Infection of these cells in turn causes a rapid disruption of blood vessels and virus dissemination to neighbouring cells, including cells in the brain (Ludwig et al., 2011). It was therefore used as a positive control to visualize BBB disruption.

To visualize the vascular endothelium, we inoculated *fli1a: GAL4FF/5xUAS:RFP* transgenic fish (hereafter referred to as *fli:G/U:RFP*), which express RFP in all endothelial cells. Live or fixed SINV-infected larvae were imaged using confocal microscopy. Given that CHIKV is of a higher biosafety level, CHIKV-infected larvae were fixed and immunolabelled with anti-GFP and anti-RFP antibodies before confocal imaging. Likewise, for IHNV, which does not include a fluorescent reporter, larvae had to be fixed and immunolabelled using a monoclonal antibody (mAb) directed against the G protein of IHNV.

Live imaging of SINV-infected larvae did not reveal any infection of endothelial cells of the BBB (Fig. 3A,B). Sometimes, intense infection of the parenchyma at 2 dpi or later made it difficult to ascertain that adjacent RFP-positive (RFP⁺) cells did not express GFP (Fig. 3B'; Movie 1); however, in that case, imaging of the same larvae at an earlier stage of infection (1 dpi) clearly showed that at this crucial time, no endothelial cell was infected (Fig. 3A'; Fig. S1A; Movie 2). The vascular network was not perturbed in SINV-infected fish (compare Fig. 3B",C"), as was verified up to 7 dpi (not shown). The same conclusions were reached by imaging fixed SINV-infected larvae. To ensure optimal imaging of deep

brain vessels, some larvae were processed using the recently developed CLARITY protocol (Chung et al., 2013; Yang et al., 2014) and then entirely imaged at high resolution. Again, imaging revealed no apparent disruption of brain microvasculature in SINV-infected animals. Infected cells were sometimes adjacent to cells of the vasculature, especially in the periphery, but no co-localization was observed (for 15 animals examined in the brain, in three independent experiments, and for 13 animals examined in the periphery; Fig. S1C'–C"; Movie 3).

By contrast, infected endothelial cells were detected in the brain vasculature of every CHIKV-infected larva at 1 or 2 dpi (Fig. 3D,E; Fig. S1B; Movie 4). The vascular network looked intact, consistent with our previous measurement of the kinetics of death of infected cells (Palha et al., 2013), which usually occurred between 2 and 3 dpi for endothelial cells in the periphery.

Finally, with IHNV, all stained fish showed many disrupted vessels (Fig. 3F; Movie 5), confirming that an abnormal vascular pattern is readily observable with these imaging conditions.

To rule out the possibility that SINV infection could loosen the BBB without direct endothelial cell infection, and thus allow leakage of virus to the brain, we performed a dye exclusion experiment on IHNV- and SINV-infected larvae. Again, because CHIKV is a Biosafety Level 3 pathogen, these experiments requiring *in vivo* imaging were not performed on CHIKV-infected larvae. We injected fluorescein isothiocyanate (FITC)-dextran (10 kDa) IV at 1 and 2 dpi and measured the relative fluorescence intensity (FI) between the brain parenchyma (BP) and the cerebral blood vasculature (CBV). Our measurements showed a significant increase in FI in the BP of IHNV-infected larvae but not in that of SINV-infected larvae (Fig. 4). Thus, the tightness of the BBB is not detectably compromised in SINV-infected larvae.

In conclusion, our data show that SINV does not infect or disrupt the BBB endothelium to gain access to the CNS. CHIKV, on the contrary, systematically infects endothelial cells of the vasculature, thus gaining an access route to the nearby parenchyma.

Macrophages play no role in entry of SINV or CHIKV into the CNS

A second possible mechanism by which viruses can enter the CNS is the so-called 'Trojan horse' strategy, where viruses infect macrophages, monocytes, or both, and exploit their natural ability to cross the BBB. To test this possibility, we used *mpeg1: GAL4FF/UAS-E1b:Eco.NfsB-mCherry* transgenic larvae (hereafter called *mpeg:G/U:NfsB-mCherry*). In this transgenic line, macrophages

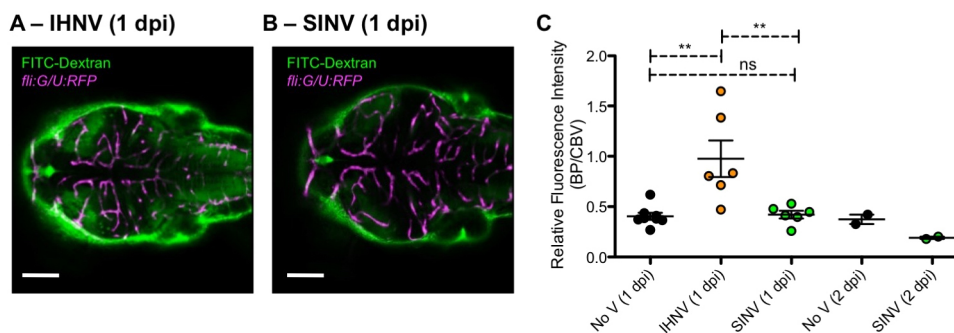


Fig. 4. SINV does not induce BBB leakage. *In vivo* assay for BBB permeability. Uninfected controls, IHNV- and SINV-infected *fli:G/U:RFP* larvae were injected IV at 1 and 2 dpi with 10 kDa FITC-dextran. One hour later, live confocal imaging of the brain was performed, to compare FITC intensity within the CBV and BP. (Injections at 2 dpi were performed only on uninfected controls and SINV-infected larvae, because of early death of IHNV-infected larvae.) (A,B) Representative images of IHNV-infected (A) and SINV-infected (B) larvae; single confocal plane at same depth. Scale bars: 100 μ m. (C) Ratios of FITC fluorescence intensities measured in BP and CBV. $n=2$ –5 larvae per group; two separate focal planes per larva.

(including microglia) express a cytosolic red fluorescent protein fused to a bacterial nitroreductase, thus allowing both fluorescence imaging of macrophages and their depletion upon addition of metronidazole to the water, as previously described (Davison et al., 2007).

Confocal microscopy after SINV or CHIKV infection of *mpeg:G/U:Nfsb-mCherry* larvae, without macrophage depletion, revealed no cell with co-localization of green and red fluorescence (for 11 SINV-infected animals examined, in four independent experiments, and for seven CHIKV-infected animals examined, in two independent experiments; Fig. 5A,B); thus macrophages were not productively infected by either virus. They displayed their characteristic contorted shape and showed no evidence of apoptosis.

We then depleted macrophages before infection by addition of metronidazole from 2 to 3 dpf. This results in a deep macrophage depletion that lasts in the periphery and CNS for at least 2 days (Fig. 5C). A progressive recovery then occurs, first observed in the caudal haematopoietic tissue, as we documented previously (see Fig. S5D of Palha et al., 2013). Macrophage-depleted SINV-infected larvae displayed a slight increase in disease severity

(disease score 5.2 ± 1.1 compared with 3.6 ± 1.0 in controls; mean \pm s.e.m.; $n=24$ per group; see Materials and Methods) but no significant increase in mortality (data not shown), in a very similar fashion to what had been observed with CHIKV (Palha et al., 2013). When CNS infection was specifically assessed, it clearly occurred in macrophage-depleted larvae, both with SINV and CHIKV. By 7 dpi, both controls and treated fish displayed a similar rate of infection ($\sim 50\%$) in the CNS upon SINV infection. In the case of CHIKV, already at 3 dpi, 100% of larvae displayed CNS infection in both controls and treated fish (Fig. 5D).

We could therefore exclude the possibility that macrophages play a significant role in the entry of either SINV or CHIKV into the CNS.

Evidence for efficient axonal transport of SINV

Several viruses infect and replicate in peripheral nerves (Koyuncu et al., 2013), which are connected to neurons of the CNS and act as a springboard for efficient entry and replication in the brain. In the case of SINV infection, we sometimes observed infection of peripheral neurons, such as trigeminal ganglion (TG) cells (Fig. 2E). However,

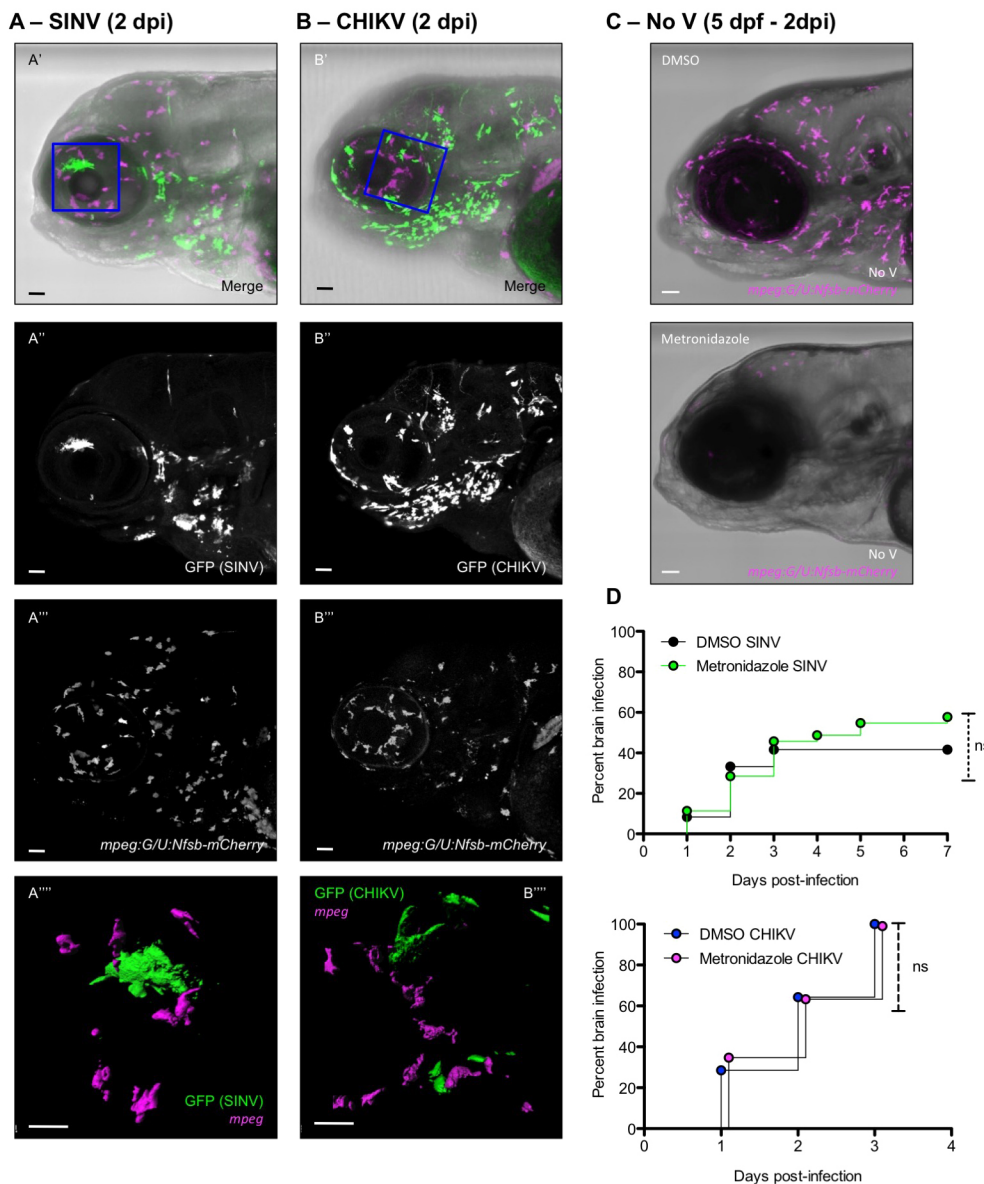


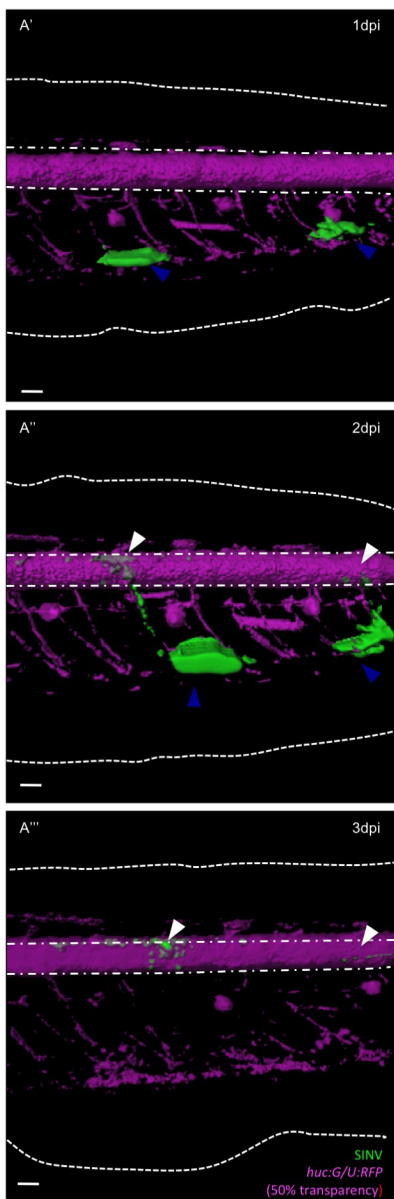
Fig. 5. Macrophages are not infected by SINV or CHIKV and not required for neuroinvasion. (A,B) Whole-mount immunohistochemistry of SINV-infected (A) or CHIKV-infected (B) *mpeg:G/U:Nfsb-mCherry* (macrophages in magenta) larva at 2 dpi. Lateral views of the head; confocal imaging, maximal projection. (A',B') Merge of transmitted light with green (infected cells) and magenta (macrophages) fluorescence. (A'',B'') Green fluorescence showing infected cells. (A''',B''') Magenta fluorescence showing macrophage distribution. (A''',B''') Magnification of the area boxed in A' and B'; green and magenta fluorescence, 3D rendering slightly tilted. Scale bars: 50 μ m (A'-A''',B'-B'''), 25 μ m (A''',B'''). (C) Macrophage depletion in *mpeg:G/U:Nfsb-mCherry* larvae. Superposition of transmitted light and magenta (macrophage) fluorescence, maximal projection, lateral view of the head, in a DMSO-treated control (top) or 2 days after treatment with metronidazole (bottom). (D) Impact of macrophage depletion on occurrence of neuroinvasion. *mpeg:G/U:Nfsb-mCherry* larvae were treated with DMSO or metronidazole, before injection with SINV (top graph) or CHIKV (bottom graph). Percentage of brain-infected larvae. $n=36$ from three independent experiments pooled. ns, not significant (Log-rank test).

because of the vast area innervated by the TG and other head ganglions, and the complexity of their connections to the brain, it was difficult to identify the sequence of events. By contrast, the spinal cord invasion offered a more tractable system. Early infection of muscle cells followed by appearance of GFP⁺ cells among motor or sensory neurons at the corresponding level of the spinal cord (Fig. 6A) was a common occurrence (observed in 44 out of 57 larvae with muscle infection, examined twice a day under the fluorescence stereomicroscope; pooled data from four independent experiments). These observations strongly suggest axonal spreading of SINV from the periphery to the CNS. By contrast, although infection of muscle fibres occurs occasionally with CHIKV, no infection of the spinal cord was observed with this virus, unless specifically injected there (not shown).

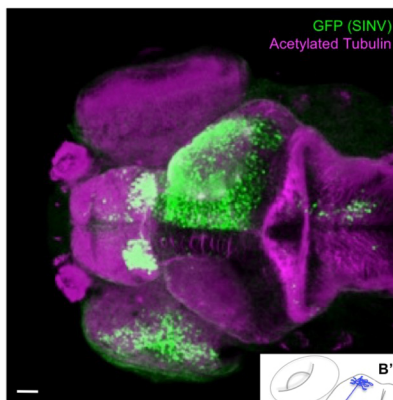
To investigate axonal transport, we injected SINV or CHIKV into the retina, between the ganglion cell layer and the outer nuclear layer (Fig. 1A), to take advantage of the well-known connectivity of the visual system (Grove, 2008; see scheme, Fig. 6B'). Fish injected in

the eye did not show an increase in mortality, and overall disease scores were comparable to those of IV-inoculated fish (data not shown). We could not prevent some leakage of the inoculum into other tissues, which resulted in infection of areas close to the injected eye. Axonal transport resulted instead in infection of the contralateral optic tectum (Fig. 6B). All SINV-infected larvae ($n=36$) displayed GFP in the retina at 1 dpi, leading to infection of the contralateral optic tectum for 45% of the injected fish. In addition, spreading of infection to other brain structures, such as the habenula in Fig. 6B, were often observed. By contrast, ~40% of CHIKV eye-injected larvae showed contralateral optic tectum infection, but of a lesser magnitude than for SINV infections (Fig. 6C). In this case, the foci of infection remained small, with no obvious spread to other CNS areas; quantification of infected areas showed a roughly tenfold decrease in efficiency of optic tectum invasion by CHIKV compared with SINV (Fig. 6D). Thus, SINV propagates efficiently, and CHIKV much less so, via axonal transport upon intraocular injection.

A – SINV - timecourse



B – SINV (2 dpi)



C – CHIKV (2 dpi)

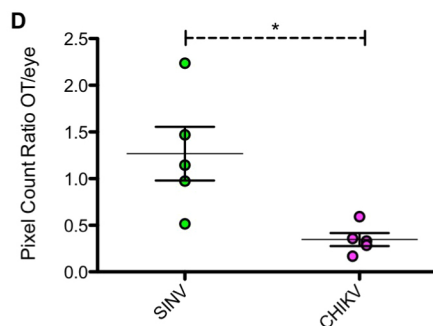
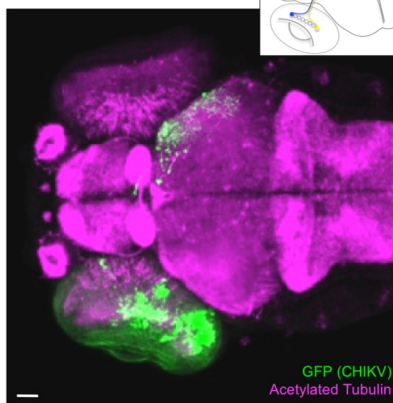


Fig. 6. Efficient axonal transport of SINV.

(A) Infection of muscle cells and connected spinal cord neurons in the tail region of a *huc:G/U:RFP* larva. Live confocal imaging, maximal projection, 3D rendering, with superposition of green (infected cells) and magenta (neurons) fluorescence. Same larva imaged at 1 (A'), 2 (A'') and 3 dpi (A'''). Dotted white lines indicate the limits of the fins; dash-dotted lines the limits of the spinal cord. Scale bars: 50 μ m. (B,C) Assay for axonal transport to the contralateral optic tectum after inoculation of SINV (B) or CHIKV (C) in the left retina. Confocal imaging of fixed infected larva at 2 dpi, with superposition of green (infected cells) and magenta (acetylated tubulin) fluorescence; maximal projections. Scale bars: 50 μ m. (B') Scheme of the projection of the retinal neurons to the optic tectum. (D) Ratio of GFP fluorescence intensities measured in the eye and the contralateral optic tectum, after SINV or CHIKV inoculation. $n=5$ from two independent experiments pooled.

Mechanisms of entry of other virus strains

We tested the generality of our findings using a different strain of each virus.

The clinical CHIKV-115 strain, which bears no fluorescent reporter gene, harbours four differences in protein sequence compared with CHIKV-GFP, including the A226V mutation in E1, shown to affect vector specificity (Tsetsarkin et al., 2007). The two viruses were known to replicate in a similar manner in zebrafish (Palha et al., 2013). The SINV339-mCherry strain, encoding a red fluorescent reporter, has eight amino acid differences compared with SINV-GFP, including the H55Q change in E2, linked to attenuation in mice (Lustig et al., 1988). It was more virulent in zebrafish than the SINV-GFP strain (Fig. S2A,B) and was therefore inoculated at a lower dose (~10 PFU) for comparison of tropism.

We infected *flila:eGFP* transgenic larvae, which express GFP in endothelial cells, with either SINV339-mCherry or CHIKV-115. We fixed the larvae at 1 and 2 dpi, and imaged the entire brain by confocal microscopy after immunolabelling. SINV339-mCherry (unlike SINV) reached the CNS in 100% of infected larvae; however, no co-localization was observed between infected cells and endothelial cells (Fig. S2C). CHIKV-115, detected with an anti-capsid antibody, was systematically observed in some brain microvessel endothelial cells, despite the lower signal given by the anti-capsid antibody used (Fig. S2D).

Altogether, the analysis of the possible CNS entry routes indicates infection of the BBB endothelium as the main route of entry of CHIKV, whereas SINV would preferentially enter via infection of peripheral nerve termini and axonal transport.

DISCUSSION

Invasion of the CNS is a key event during many viral infections and often a matter of life or death for the host. It is, however, difficult to follow this phenomenon in mammals, hindering the design of preventive strategies.

In the present work, we used zebrafish to characterize the infection course of SINV, a well-established model for the study of viral encephalitis. We focused on its neuroinvasion and compared it with that of CHIKV. This was studied following IV injections, which mimic the natural entry route of these mosquito-transmitted viruses, even though it results in more inter-individual variability than direct IC inoculation. We found that, upon IV inoculation of SINV, infected cells appeared in the periphery as early as 8 hpi, always before infected neurons of the CNS. Infection spontaneously declined in the periphery, probably as a result of the host response. Indeed, qRT-PCR analysis of whole larvae revealed strong induction of type I interferon (IFN) and IFN-stimulated genes of an amplitude and kinetics comparable to those elicited by CHIKV (not shown; a detailed analysis of the response will be reported in a separate publication). By contrast, infection persisted in the CNS. Overall, the disease signs and kinetics of SINV infection in zebrafish were similar to those previously observed in CHIKV-infected fish (Palha et al., 2013), suggesting that many of the mechanisms that determine disease onset might be conserved between related Alphaviruses. However, the entry and spread in the CNS differed. CNS entry of CHIKV was more frequent than for SINV (100 vs 50%), but then SINV infection of the CNS was more active, increasing in size and advancing to other brain areas. This is consistent with the different routes of CNS entry suggested by our study: via infection of endothelial cells of the BBB for CHIKV, and via infection of peripheral nerves and peripheral transport for SINV.

What routes of access to the CNS could have been used by these viruses apart from the three we tested? Direct access via an

immature, leaky BBB can be dismissed. Fleming et al. (2013) characterized the progressive maturation of the BBB in zebrafish. At 3 dpf, the time at which larvae were injected, medium molecular weight molecules (~900 Da) are already blocked from entry into the CNS (Fleming et al., 2013), thus excluding passive transport of the much bigger (52 MDa) viral particles from the blood. In some cases, viruses have been shown to enter via the choroid plexus (ChP) (e.g. HIV; Falangola et al., 1995), the region of the brain where the cerebrospinal fluid is formed. Studies on morphogenesis have shown that in zebrafish the ChP develops at the dorsal midline on the fourth ventricle and shifts towards the ear level at ~3 dpf (García-Lecea et al., 2008). Here we found that commonly infected areas in the brain were rather lateral or distant from the ChP (e.g. olfactory bulb, optic tectum, medulla), which strongly suggests that neither SINV nor CHIKV enters the brain via prior infection of the forming ChP.

In the case of SINV, the vasculature was shown to remain intact. Moreover, infection of endothelial cells of the brain microvessels was never observed. Injection of a dye confirmed the integrity of the BBB, as leakage into the brain parenchyma did not occur in SINV-infected larvae. IC injections revealed little or no infection of cells outside the CNS, thereby corroborating the observation that SINV does not compromise the integrity of the BBB. CHIKV was, on the contrary, capable of infecting endothelial cells of both the periphery and the brain microvasculature, thus gaining an easy access to brain parenchyma. Biosafety-imposed limitations to live imaging of CHIKV infection have so far precluded direct imaging of the progression of CHIKV infection from the vasculature to the adjacent brain parenchyma, but that is an objective we will be pursuing.

Importantly, when we tested different strains of either SINV or CHIKV, the key property of infection of brain endothelial cells was conserved. Unexpectedly, the SINV339-mCherry strain was found to be significantly more virulent than its GFP counterpart. This was unexpected because the TE12 strain, on which the GFP virus is based, possesses the envelope genes from the more virulent NSV strain (Lustig et al., 1988). However, as NSV had been derived from AR339 by IC passages in mice, these virulence determinants might very well be mouse specific. Alternatively, this could also be attributable to the different position of the fluorescent reporter gene, which also has an influence on virulence (Sun et al., 2014). This is an issue that we are currently investigating. Nevertheless, we showed that irrespective of the strain used, SINV and CHIKV differ in their CNS cell tropism, which in turn determines their different mechanisms of entry into the CNS.

We also showed that neither SINV nor CHIKV targets macrophages. Macrophage depletion assays induced a slightly higher disease severity in treated fish, as in the CHIKV model, but did not prevent the virus from accessing the CNS. These results show that, even though macrophages might contribute in part to the control of SINV infection, they are not required for the virus to reach the CNS.

The observations we collected from SINV-inoculated larvae therefore strongly support the hypothesis that viral entry into the CNS occurs after infection of peripheral nerves. We observed, in some cases, infection of TG neurons that innervate the head and are connected to the brain, or infection of muscle cells followed by infection of corresponding motoneurons. These results are in accordance with the aforementioned study of mice infected with a luciferase-recombinant SINV strain, where viral replication in the nose or the spinal cord was shown always to precede infection in the brain (Cook and Griffin, 2003). Our eye inoculation experiments

also showed that SINV, much more than CHIKV, can be transported efficiently by axons; a feature that is also consistent with the progressive spread to several brain substructures commonly observed with SINV infection. Our next challenge will be to achieve *in vivo* imaging of virions and of axonal transport of the virus, which will require prolonged development of new tools.

Understanding the entry mechanism of a certain pathogen into the CNS has always been hindered by the difficulties in visualizing the progression of the infection. Moreover, high numbers of animals and organ/tissue samples are generally needed at different time points to avoid missing important cues. The combined use of recombinant virus strains with fluorescent-reporter zebrafish lines, on the contrary, allowed us to gain single-cell resolution details at the whole organism level and with minimal invasiveness for the host over the full course of infection. The characterization of two viruses that rely on different entry routes to the CNS, along with future study of other neurotropic viruses in zebrafish, provides a powerful tool to test new antiviral therapeutics *in vivo*.

MATERIALS AND METHODS

Ethical statement

Animal experiments were conducted according to European Union guidelines for handling of laboratory animals (http://ec.europa.eu/environment/chemicals/lab_animals/home_en.htm). All protocols were approved by the Ethical Committee for Animal Experimentation of Institut Pasteur – CEEA 89 and the French Ministry of Research and Education (permit #01265.03). During injections or live imaging sessions, animals were anaesthetized with tricaine (Sigma-Aldrich, A-5040); at the end of the experimental procedures, they were euthanized by anaesthetic overdose.

Fish lines and husbandry

Zebrafish embryos were raised according to standard procedures as previously described (Westerfield, 2000; Levraud et al., 2008). WT AB zebrafish were initially obtained from ZIRC (Eugene, OR, USA). The following transgenic and mutant lines were also used: Tg(*elavl3:Gal4*)^{z349} (Akerboom et al., 2012), Tg(*fli1a:Gal4FF*)^{ubs4} (Zygmunt et al., 2011), Tg(*5xUAS:RFP*)^{nkuastrfp1a} (Asakawa et al., 2008), Tg(*mpeg:Gal4FF*)^{g125} (Ellett et al., 2011), Tg(*UAS-E1b:Eco.NfsB-mCherry*)^{z264} (Davison et al., 2007) and Tg(*fli1a:eGFP*)^{y1} (Lawson and Weinstein, 2002). Owing to silencing issues of some UAS-driven transgenes, breeders were carefully screened to select those whose progeny yielded full expression; correct fluorescence expression by larvae was checked before experiments.

Eggs obtained by natural spawning were bleached and raised at 28°C in Volvic source water. Eggs were raised in 1-phenyl-2-thiourea (PTU)/Volvic (Sigma-Aldrich; 0.003% final) from 24 hpf onwards to prevent melanin pigment formation. In control experiments, we verified that overall viral replication (measured by qRT-PCR) and the frequency of brain infection remain unchanged in the absence or presence of PTU. At 3 dpf, immediately before infections, larvae that had not hatched spontaneously were manually dechorionated.

Viruses

SINV and CHIKV viruses were produced on BHK cells [originally obtained from American Type Culture Collection (ATCC), #CC-L10], according to Hardwick and Levine (2000). The SINV-GFP backbone is from the hybrid TE12 strain, with non-structural and capsid regions from the laboratory-adapted Toto1101 strain and most of the envelope region from the NSV strain isolated after six intracerebral passages of AR339 in mice (Lustig et al., 1988). It harbours a 3' genomic insertion of the eGFP gene under the control of a second subgenomic promoter (Hahn et al., 1992). The SINV339-mCherry backbone comes from the low-passage AR339 strain, with a self-cleavable mCherry inserted between the capsid and pE2 regions (Sun et al., 2014). CHIKV-GFP corresponds to the CHIKV-LR 5' GFP virus

of Tsetsarkin et al. (2006). It contains an insertion of the GFP-encoding sequence between the two main open reading frames of CHIKV under the control of an additional subgenomic promoter. The LR backbone used (#EU224268) derives from the OPY1 strain, a 2006 clinical isolate from La Réunion. CHIKV-115 is another clinical isolate from La Réunion (Schuffenecker et al., 2006) (#AM258990). Heat-adapted IHNV strain 25.70 was produced on EPC cells (ATCC #CRL-2872) as described previously (Ludwig et al., 2011).

Injections and disease scores

Injections and handling of larvae were performed as described by Levraud et al. (2008). Briefly, zebrafish larvae aged 70-72 hpf were inoculated by microinjection of ~10² PFU viral SINV or CHIKV particles (~10 PFU in the case of SINV339-mCherry) (~1 nl of supernatant from infected BHK cells, diluted with PBS to 10⁸ PFU/ml). Injections were performed in the caudal vein or aorta (IV) or in the left optic tectum (IC) or in the left retina (eye) (Fig. 1A). Larvae were then distributed in individual wells of 24-well culture plates with 1 ml water containing PTU, kept at 28°C and inspected at least daily with a stereomicroscope until 7 dpi. Clinical signs of infection were assessed first on aware animals, which were then anaesthetized for better observation. Quantitative assessment of the clinical status was based on a precise list of criteria, as previously described (Palha et al., 2013). Briefly, clinical signs were assessed blindly, yielding a disease score ranging from 0 (no disease sign) to 15 (dead or terminally ill). The signs evaluated included the following: ability to maintain equilibrium (on 1 point), response to touch, body shape, blood flow, cardiac rhythm, presence of oedema, inflation of the swim bladder, and opacity of the yolk (each on 2 points). For ethical reasons, all larvae used in the experiments were euthanized by anaesthetic overdose at 7 dpi.

IHNV infections were performed as described by Ludwig et al. (2011). Briefly, larvae were injected IV with 10² PFU of IHNV25.70, distributed in individual 24-well plates and incubated at 24°C.

Injections of FITC-dextran (10 kDa; Sigma) were performed at 2 dpi on control uninfected larvae, IHNV- and SINV-infected larvae. Larvae were imaged 1 h post-injection (see below).

Viral titrations

SINV-infected larvae were anaesthetized and homogenized at 2 dpi. Dilutions of homogenate supernatant were prepared in serum-free Dulbecco's modified Eagle's medium (DMEM) and used to inoculate confluent monolayers of Vero-E6 cells (ATCC #CRL-1586) for between 30 min and 1 h at 37°C. Cells were then overlaid with 0.8% agarose in DMEM containing 1.6% newborn calf serum. Samples were incubated for 48 h. Following incubation, cells were fixed with 4% formalin and revealed with Crystal Violet solution [10% Crystal Violet (Sigma), 20% ethanol]. Plaques were enumerated and used to back-calculate the number of PFU per larva.

In vivo confocal imaging

For *in vivo* imaging, 5-10 larvae were anaesthetized with 112 µg/ml tricaine and immobilized in ~1% low-melting-point agarose in the centre of a 35 mm glass-bottomed Ibidi dish, then covered with ~2 ml water containing tricaine. Transmitted light/fluorescence imaging was performed using a Leica SPE inverted confocal microscope using a 10× ACS APO dry objective (NA 0.30). Imaging was typically performed at 26°C, with 2 µm step z-stacks. Fish were imaged every day beginning at 1 dpi up to 4-5 dpi, with imaging sessions typically lasting 10-15 min; control uninfected larvae were always included.

Whole-mount immunohistochemistry and imaging of fixed samples

Zebrafish larvae from 4 to 7 dpf were fixed in freshly prepared formaldehyde 4% (wt/vol; in PBS) overnight at 4°C. Fixed samples were washed twice in PBS containing 0.1% Tween 20 (PBSt), and whole-mount immunohistochemistry was performed as described by Svoboda et al. (2001). The following primary antibodies were used: chicken polyclonal to GFP (Abcam, ab13970, 1:500); mouse mAb to acetylated tubulin (Sigma,

T7451, 1:1000); rabbit polyclonal to DsRed (Clontech, 632496, 1:500), which also labels the mCherry protein; 19B7 mouse mAb antibody specific against IHN V G protein (1:500) (Biacchesi et al., 2002); and a mouse mAb to Alphavirus capsid (1:200) (Greiser-Wilke et al., 1989). Secondary antibodies used were as follows: Alexa 488-labelled goat anti-chicken (Invitrogen, A11039, 1:500); Alexa Cy3-labelled goat anti-mouse (Jackson ImmunoResearch, 115-166-003, 1:500); Alexa Cy5-labelled goat anti-mouse (Jackson ImmunoResearch, 115-176-072, 1:500); and Cy3-labelled goat anti-rabbit IgG (Jackson ImmunoResearch, 115-166-003, 1:500). Nuclei were stained for 45 min at room temperature with DAPI in PBSt (Sigma; 5 mg/ml). Fixed embryos were progressively transferred into 80% glycerol before imaging. Images were acquired with the Leica SPE inverted confocal microscope, using a 10× dry ACS APO objective (NA 0.30) or a 40× ACS APO oil immersion objective (NA1.15) for subregions (e.g. Fig. 2E), and z-stacks of a maximum of 150 μm in 2 μm steps were obtained. Image processing (maximal projections and reconstruction of whole embryos) was carried out with Adobe Photoshop CS6 software. 3D rendering of confocal stacks was done using BitPlane Imaris software, using default parameters except that red colour transparency was set at 50%.

Passive clarification (CLARITY)

Zebrafish larvae at 4–7 dpf were fixed and washed as previously described. Samples were then infused in a precooled (4°C) solution of freshly prepared hydrogel monomers [0.01 M PBS, 0.25% VA-044 initiator (wt/vol), 5% dimethyl sulphoxide (DMSO; vol/vol), 1% paraformaldehyde (wt/vol), 4% acrylamide (wt/vol) and 0.0025% bis-acrylamide (wt/vol)] for 2 days at 4°C. After degassing the samples, the hydrogel polymerization was triggered by replacing atmospheric oxygen with nitrogen in a desiccation chamber for 3 h at 37°C. Samples were cleaned from superfluous hydrogel and transferred into embedding cassettes for lipid clearing. Passive lipid clearing was performed for 5 days at 40°C in the clearing solution [8% SDS (wt/vol), 0.2 M boric acid, pH adjusted to 8.5] under gentle agitation. Subsequently, the samples were thoroughly washed in PBSt for 2 days at room temperature with gentle agitation.

Immunostaining of clarified samples

CLARITY-processed larvae were incubated in blocking solution [0.01 M PBS, 0.1% Tween 20 (vol/vol), 1% Triton X-100 (vol/vol), 10% DMSO (vol/vol), 10% normal goat serum (vol/vol), 0.05 M glycine] overnight at 4°C. Subsequently, samples were incubated in staining solution [0.01 M PBS, 0.1% Tween 20 (vol/vol), 0.1% Triton X-100 (vol/vol), 10% DMSO (vol/vol), 2% normal goat serum (vol/vol), 0.05% azide (vol/vol)] with primary antibodies [chicken polyclonal to GFP (Avès Labs, GFP-1010, 1:600); rabbit polyclonal to DsRed (Clontech, 632496, 1:300)] for 5 days at room temperature under gentle agitation. After four washing steps in PBSt, samples were incubated in staining solution with secondary antibodies [Alexa Fluor 488-labelled goat anti-chicken (Invitrogen, A11039, 1:600); Alexa 555-labelled goat anti-rabbit (Invitrogen, A-21428, 1:300)] for 5 days at room temperature. Samples were washed for 2 days in PBSt and stained with 1 μM DiI18(3) solution (DiI Stain; Molecular Probes).

Imaging of clarified samples in high refractive index solution

A fructose-based high refractive index solution (fbHRI) was prepared as follows: 70% fructose (wt/vol), 20% DMSO (wt/vol) in 0.002 M PBS, 0.005% sodium azide (wt/vol). The refractive index of the solution was adjusted to 1.4571 using a refractometer (Kruss). In preparation for imaging, the samples were incubated in 50% (vol/vol) fbHRI for 6 h and finally incubated in fbHRI for at least 12 h. For imaging, samples were mounted in 1% (wt/vol) low-melting-point agarose and covered with fbHRI. Fluorescence of whole-mount larvae was recorded with a Leica TCS SP8 two-photon microscope equipped with a mode-locked Ti:Sapphire laser (Chameleon, Coherent) at 770 nm and the Leica HC FLUOTAR L 25×/1.00 IMM motCorr objective.

Quantification of BBB leakage *in vivo*

The confocal images taken after IV dextran-FITC injection were analysed using ImageJ (<http://imagej.nih.gov/ij/>) as previously described (Watanabe et al., 2012). For each larva, two separate focal planes were selected. In each

plane, five circular regions of interest (ROI) 15 μm in diameter were selected in the BP outside the CBV. Twenty single-pixel ROIs were selected in the CBV. The FI was calculated for each ROI (circular and single pixel) as well as the relative FI (BP/CBV).

Quantification of GFP infection levels in eye-injected larvae

The confocal images taken after injection of SIN V or CHIKV into the eye were analysed using ImageJ. For each larva, two ROI were selected: the eye, and the contralateral region of the optic tectum. A threshold was applied to each ROI, to remove background noise (e.g. autofluorescence coming from the pigments in the eye). Infection levels were calculated as the ratio between GFP in the optic tectum and the eye.

Macrophage depletion

Metronidazole-mediated depletion was performed as described by Palha et al. (2013). Briefly, Tg(*mpeg:Gal4FF*)^{g125} fish (Ellett et al., 2011) were crossed with Tg(*UAS-E1b:Eco.Nf̄sB-mCherry*)^{c264} (Davison et al., 2007) to generate double-positive transgenics and single-positive sibling controls. Embryos were placed from 48 to 72 hpf in a 10 mM metronidazole, 0.1% DMSO solution to induce specific depletion of Nf̄sB-mCherry-expressing macrophages. Embryos were then rinsed three times with embryo water and subsequently injected with the virus.

Statistical analysis

To evaluate the difference between means, a two-tailed unpaired *t*-test or an analysis of variance (ANOVA) followed by Bonferroni's multiple comparison test were used, when appropriate. Normal distributions were analysed with the Kolmogorov–Smirnov test. Non-Gaussian data were analysed with a Kruskal–Wallis test followed by Dunn's multiple comparison test. A value of *P*<0.05 was considered statistically significant (***P*<0.001; **P*<0.01; **P*<0.05; ns, not significant). Survival data were plotted using the Kaplan–Meier estimator, and log-rank tests were performed to assess differences between groups. Statistical analyses were performed using Prism 5 software (GraphPad).

Acknowledgements

We wish to thank Benjamin Obadia for SIN V suspensions and plasmids, Barbara Rizzi for 3D reconstruction of *fli:G/U:RFP* larvae, Paolo Di Marco for his help with image analysis and processing, Arnim Jenett for the generation of the multi-panel movies, Florence Guivel-Benhassine and Olivier Schwartz for sharing protocols and the anti-CHIKV capsid antibody, Aurélie Lunazzi and Maxence Frétaud for technical assistance, Franck Bourrat for sharing his expertise in neuroanatomy, Emma Colucci-Guyon and Pedro Hernández for critical reading of the manuscript, and Jose Perez and Johann Rolin for their invaluable care of the fish facility.

Competing interests

The authors declare no competing or financial interests.

Author contributions

Conceptualization: C.L., N.P., P.B., J.-P.L.; Methodology: G.P., C.L., P.A., J.-S.J., J.-P.L.; Validation: G.P., J.-P.L. Formal analysis: G.P., C.L., V.B., P.A.; Investigation: G.P., N.P., B.C.M., V.B., P.A., E.D.J., J.-P.L.; Resources: M.V., M.S., P.H.; Writing - original draft: G.P., C.L., P.B., J.-P.L. Writing - review & editing: G.P., C.L., N.P., B.C.M., P.A., J.-S.J., M.S., P.B., J.-P.L.; Visualization: G.P., P.A., E.D.J.; Supervision: C.L., J.-S.J., P.B., J.-P.L.; Project administration: P.B., J.-P.L.; Funding acquisition: M.V., P.H., P.B., J.-P.L.

Funding

This work was supported by funding from the European Community's Seventh Framework Programme [FP7-PEOPLE-2011-ITN] under grant agreement no. PITN-GA-2011-289209 for the Marie Curie Initial Training Network FishForPharma; the Agence Nationale de la Recherche (Zebraflam grant ANR-10-MDI-009); a Domaine d'Interet Majeur Maladies Infectieuses (DIM-Malinf) grant from Région Ile-de-France; institutional support was from Institut National de la Recherche Agronomique (INRA), the Institut Pasteur and Centre National de la Recherche Scientifique. This work also benefited from the facilities and expertise of TEFOR – Investissement d'avenir – ANR-II-INBS-0014.

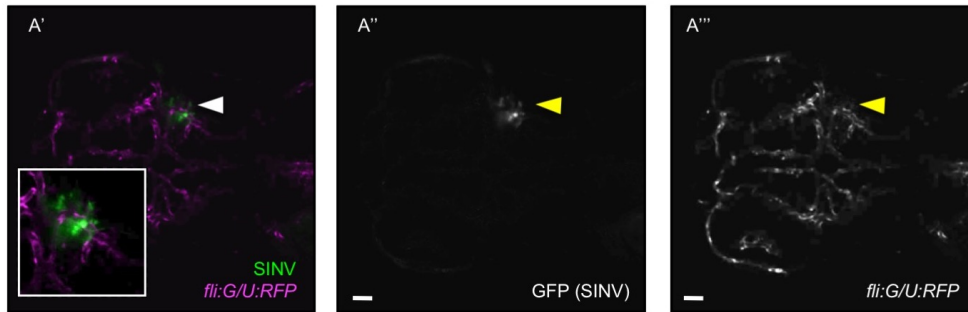
Supplementary information

Supplementary information available online at <http://dmm.biologists.org/lookup/doi/10.1242/dmm.029231.supplemental>

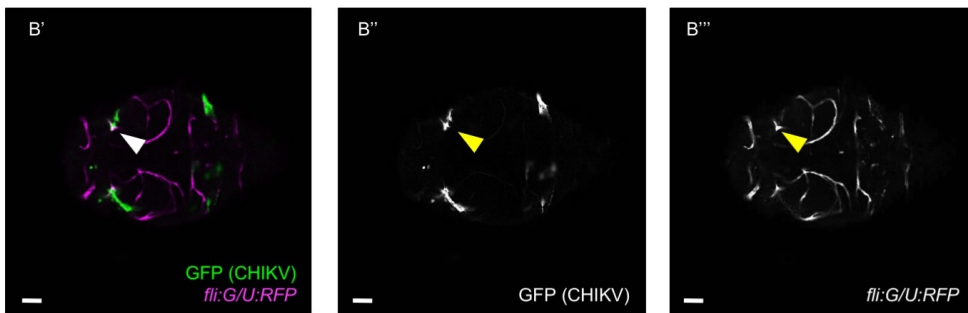
References

- Akerboom, J., Chen, T.-W., Wardill, T. J., Tian, L., Marvin, J. S., Mutlu, S., Calderón, N. C., Esposti, F., Borghuis, B. G., Sun, X. R. et al. (2012). Optimization of a GCaMP calcium indicator for neural activity imaging. *J. Neurosci.* **32**, 13819-13840.
- Arpino, C., Curatolo, P. and Rezza, G. (2009). Chikungunya and the nervous system: what we do and do not know. *Rev. Med. Virol.* **19**, 121-129.
- Asakawa, K., Suster, M. L., Mizusawa, K., Nagayoshi, S., Kotani, T., Urasaki, A., Kishimoto, Y., Hibi, M. and Kawakami, K. (2008). Genetic dissection of neural circuits by Tol2 transposon-mediated Gal4 gene and enhancer trapping in zebrafish. *Proc. Natl. Acad. Sci. USA* **105**, 1255-1260.
- Biacchesi, S., Béarzotti, M., Bouguyon, E. and Brémont, M. (2002). Heterologous exchanges of the glycoprotein and the matrix protein in a Novirhabdovirus. *J. Virol.* **76**, 2881-2889.
- Casiraghi, C., Dorovini-Zis, K. and Horwitz, M. S. (2011). Epstein-Barr virus infection of human brain microvessel endothelial cells: a novel role in multiple sclerosis. *J. Neuroimmunol.* **230**, 173-177.
- Chung, K., Wallace, J., Kim, S.-Y., Kalyanasundaram, S., Andalman, A. S., Davidson, T. J., Mirzabekov, J. J., Zalocusky, K. A., Mattis, J., Denison, A. K. et al. (2013). Structural and molecular interrogation of intact biological systems. *Nature* **497**, 332-337.
- Cook, S. H. and Griffin, D. E. (2003). Luciferase imaging of a neurotropic viral infection in intact animals. *J. Virol.* **77**, 5333-5338.
- Couderc, T., Chrétien, F., Schilte, C., Disson, O., Brigitte, M., Guivel-Benhassine, F., Touret, Y., Barau, G., Cayet, N., Schuffenecker, I. et al. (2008). A mouse model for chikungunya: young age and inefficient type-I interferon signaling are risk factors for severe disease. *PLoS Pathog.* **4**, e29.
- Das, T., Jaffar-Bandjee, M. C., Hoarau, J. J., Krejbich Trotot, P., Denizot, M., Lee-Pat-Yuen, G., Sahoo, R., Guiraud, P., Ramful, D., Robin, S. et al. (2010). Chikungunya fever: CNS infection and pathologies of a re-emerging arbovirus. *Prog. Neurobiol.* **91**, 121-129.
- Davison, J. M., Akitake, C. M., Goll, M. G., Rhee, J. M., Gosse, N., Baier, H., Halpern, M. E., Leach, S. D. and Parsons, M. J. (2007). Transactivation from Gal4-VP16 transgenic insertions for tissue-specific cell labeling and ablation in zebrafish. *Dev. Biol.* **304**, 811-824.
- Economopoulou, A., Dominguez, M., Helync, B., Sissoko, D., Wichmann, O., Quenel, P., Germonneau, P. and Quatresous, I. (2009). Atypical chikungunya virus infections: clinical manifestations, mortality and risk factors for severe disease during the 2005-2006 outbreak on Réunion. *Epidemiol. Infect.* **137**, 534-541.
- Ellett, F., Pase, L., Hayman, J. W., Andrianopoulos, A. and Lieschke, G. J. (2011). Mpeg1 promoter transgenes direct macrophage-lineage expression in zebrafish. *Blood* **117**, e49-e56.
- Falangola, M. F., Hanly, A., Galvao-Castro, B. and Petito, C. K. (1995). HIV infection of human choroid plexus: a possible mechanism of viral entry into the CNS. *J. Neuropathol. Exp. Neurol.* **54**, 497-503.
- Fleming, A., Diekmann, H. and Goldsmith, P. (2013). Functional characterisation of the maturation of the blood-brain barrier in larval zebrafish. *PLoS ONE* **8**, e77548.
- Fletcher, N. F., Wilson, G. K., Murray, J., Hu, K., Lewis, A., Reynolds, G. M., Stamatakis, Z., Meredith, L. W., Rowe, I. A., Luo, G. et al. (2012). Hepatitis C virus infects the endothelial cells of the blood-brain barrier. *Gastroenterology* **142**, 634-643.e6.
- Furuta, T., Tomioka, R., Taki, K., Nakamura, K., Tamamaki, N. and Kaneko, T. (2001). In vivo transduction of central neurons using recombinant Sindbis virus: Golgi-like labeling of dendrites and axons with membrane-targeted fluorescent proteins. *J. Histochem. Cytochem.* **49**, 1497-1508.
- García-Lecea, M., Kondrychyn, I., Fong, S. H., Ye, Z.-R. and Korzh, V. (2008). In vivo analysis of choroid plexus morphogenesis in zebrafish. *PLoS ONE* **3**, e3090.
- Greiser-Wilke, I., Moening, V., Kaaden, O. R. and Figueiredo, L. T. (1989). Most alphaviruses share a conserved epitopic region on their nucleocapsid protein. *J. Gen. Virol.* **70**, 743-748.
- Grove, E. A. (2008). Turning neurons into a nervous system. *Development* **135**, 2203-2206 (Meeting Review).
- Gubler, D. J. (2001). Human arbovirus infections worldwide. *Ann. N. Y. Acad. Sci.* **951**, 13-24.
- Hahn, C. S., Hahn, Y. S., Braciale, T. J. and Rice, C. M. (1992). Infectious Sindbis virus transient expression vectors for studying antigen processing and presentation. *Proc. Natl. Acad. Sci. USA* **89**, 2679-2683.
- Hardwick, J. M. and Levine, B. (2000). Sindbis virus vector system for functional analysis of apoptosis regulators. *Methods Enzymol.* **322**, 492-508.
- Heap, L. A., Goh, C. C., Kassahn, K. S. and Scott, E. K. (2013). Cerebellar output in zebrafish: an analysis of spatial patterns and topography in eurydendroid cell projections. *Front. Neural Circuits* **7**, 53.
- Koyuncu, O. O., Hogue, I. B. and Enquist, L. W. (2013). Virus infections in the nervous system. *Cell Host Microbe* **13**, 379-393.
- Lawson, N. D. and Weinstein, B. M. (2002). In vivo imaging of embryonic vascular development using transgenic zebrafish. *Dev. Biol.* **248**, 307-318.
- Levraud, J.-P., Colucci-Guyon, E., Redd, M. J., Lutfalla, G. and Herbomel, P. (2008). In vivo analysis of zebrafish innate immunity. *Methods Mol. Biol.* **415**, 337-363.
- Levraud, J.-P., Palha, N., Langevin, C. and Boudinot, P. (2014). Through the looking glass: witnessing host-virus interplay in zebrafish. *Trends Microbiol.* **22**, 490-497.
- Lewis, J., Wesselingh, S. L., Griffin, D. and Hardwick, M. (1996). Alphavirus-induced apoptosis in mouse brains correlates with neurovirulence. *J. Virol.* **70**, 1828-1835.
- Ludwig, M., Palha, N., Torhy, C., Briolat, V., Colucci-Guyon, E., Brémont, M., Herbomel, P., Boudinot, P. and Levraud, J.-P. (2011). Whole-body analysis of a viral infection: vascular endothelium is a primary target of infectious hematopoietic necrosis virus in zebrafish larvae. *PLoS Pathog.* **7**, e1001269.
- Lustig, S., Jackson, A. C., Hahn, C. S., Griffin, D. E., Strauss, E. G. and Strauss, J. H. (1988). Molecular basis of Sindbis virus neurovirulence in mice. *J. Virol.* **62**, 2329-2336.
- Mounce, B. C., Poirier, E. Z., Passoni, G., Simon-Lorière, E., Cesaro, T., Prot, M., Stapleford, K. A., Moratorio, G., Sakuntabhai, A., Levraud, J.-P. et al. (2016). Interferon-induced spermidine-spermine acetyltransferase and polyamine depletion restrict Zika and chikungunya viruses. *Cell Host Microbe* **20**, 167-177.
- Paessler, S. and Taylor, K. (2011). Encephalitic Development in Alphaviral Infection. In *Non-Flavivirus Encephalitis* (Ed. S. Tkachev). *InTech*, doi:10.5772/24175.
- Palha, N., Guivel-Benhassine, F., Briolat, V., Lutfalla, G., Sourisseau, M., Ellett, F., Wang, C.-H., Lieschke, G. J., Herbomel, P., Schwartz, O. et al. (2013). Real-time whole-body visualization of chikungunya virus infection and host interferon response in zebrafish. *PLoS Pathog.* **9**, e1003619.
- Powers, A. M. and Logue, C. H. (2007). Changing patterns of chikungunya virus: re-emergence of a zoonotic arbovirus. *J. Gen. Virol.* **88**, 2363-2377.
- Rameix-Welti, M.-A., Le Goffic, R., Hervé, P.-L., Sourimant, J., Rémot, A., Riffault, S., Yu, Q., Galloux, M., Gault, E. and Eléouët, J.-F. (2014). Visualizing the replication of Respiratory Syncytial virus in cells and in living mice. *Nat. Commun.* **5**, 5104.
- Schuffenecker, I., Iteman, I., Michault, A., Murri, S., Frangeul, L., Vaney, M. C., Lavenir, R., Pardigon, N., Reynes, J. M., Pettinelli, F. et al. (2006). Genome microevolution of chikungunya viruses causing the Indian Ocean outbreak. *PLoS Med.* **3**, e263.
- Sun, C., Gardner, C. L., Watson, A. M., Ryman, K. D. and Klimstra, W. B. (2014). Stable, high-level expression of reporter proteins from improved alphavirus expression vectors to track replication and dissemination during encephalitic and arthritogenic disease. *J. Virol.* **88**, 2035-2046.
- Svoboda, K. R., Linares, A. E. and Ribera, A. B. (2001). Activity regulates programmed cell death of zebrafish Rohon-Beard neurons. *Development* **128**, 3511-3520.
- Swanson, P. A. and McGavern, D. B. (2015). Viral diseases of the central nervous system. *Curr. Opin. Virol.* **11**, 44-54.
- Tsatsarkin, K., Higgs, S., McGee, C. E., De Lamballerie, X., Charrel, R. N. and Vanlandingham, D. L. (2006). Infectious clones of chikungunya virus (La Réunion isolate) for vector competence studies. *Vector Borne Zoonotic Dis.* **6**, 325-337.
- Tsatsarkin, K. A., Vanlandingham, D. L., McGee, C. E. and Higgs, S. (2007). A single mutation in chikungunya virus affects vector specificity and epidemic potential. *PLoS Pathog.* **3**, e201.
- Watanabe, K., Nishimura, Y., Nomoto, T., Umamoto, N., Zhang, Z., Zhang, B., Kuroyanagi, J., Shimada, Y., Shintou, T., Okano, M. et al. (2012). In vivo assessment of the permeability of the blood-brain barrier and blood-retinal barrier to fluorescent indoline derivatives in zebrafish. *BMC Neurosci.* **13**, 101.
- Westerfield, M. (2000). *The Zebrafish Book: A Guide for the Laboratory Use of Zebrafish (Danio rerio)*. Corvallis: University of Oregon Press.
- Xu, Z., Waeckerlin, R., Urbanowski, M. D., van Marle, G. and Hobman, T. C. (2012). West Nile virus infection causes endocytosis of a specific subset of tight junction membrane proteins. *PLoS ONE* **7**, e37886.
- Yang, B., Treweek, J. B., Kulkarni, R. P., Deverman, B. E., Chen, C.-K., Lubeck, E., Shah, S., Cai, L. and Gradinaru, V. (2014). Single-cell phenotyping within transparent intact tissue through whole-body clearing. *Cell* **158**, 945-958.
- Zhu, P., Narita, Y., Bundschuh, S. T., Fajardo, O., Schäfer, Y. P., Chattopadhyaya, B., Bouldoires, E. A., Stepien, A. E., Deisseroth, K., Arber, S. et al. (2009). Optogenetic dissection of neuronal circuits in zebrafish using viral gene transfer and the Tet system. *Front. Neural Circuits* **3**, 21.
- Zygmunt, T., Gay, C. M., Blondelle, J., Singh, M. K., Flaherty, K. M. C., Means, P. C., Herwig, L., Krudewig, A., Belting, H.-G., Affolter, M. et al. (2011). Semaphorin-PlexinD1 signaling limits angiogenic potential via the VEGF decoy receptor sFlt1. *Dev. Cell* **21**, 301-314.

A – SINV (1 dpi)



B – CHIKV (1 dpi)



C – SINV (2 dpi) CLARITY

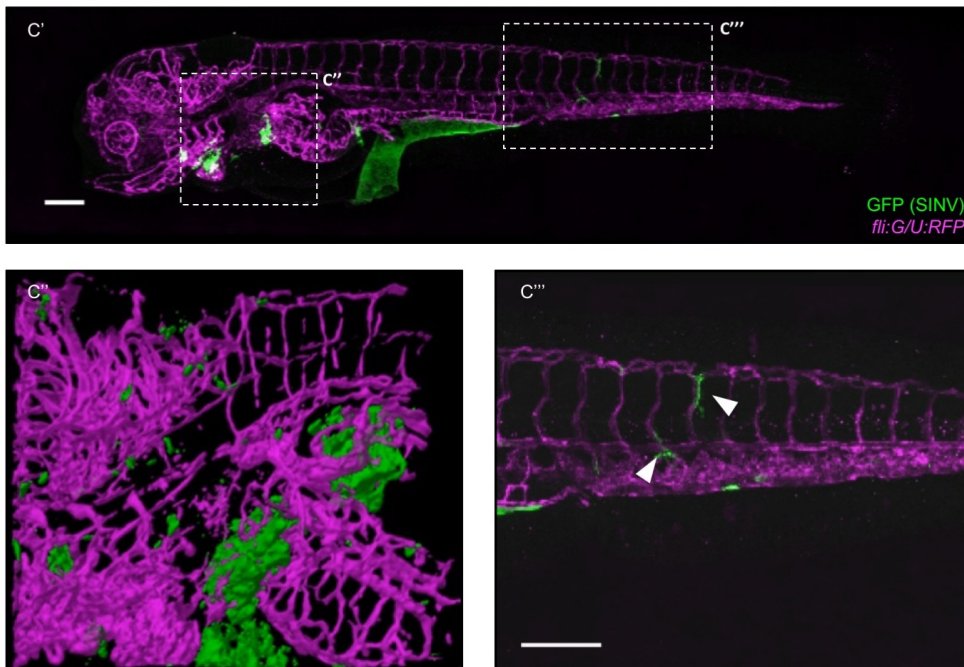


Figure S1. High magnification imaging of vasculature in infected larvae.

Confocal imaging, single focal planes extracted from Fig. (3A') and (3D'). Scale bars: 50 μ m.

(A) SINV infection live imaging, from Fig. (3A'); (A') merge of green (infected cells) and magenta (endothelium) fluorescence; (A'') green (infected cells) fluorescence; (A''') magenta (endothelium) fluorescence. White and yellow arrowheads: infected areas close to but not part of the vasculature.

(B) CHIKV infection, fixed sample labeled for GFP and RFP, from Fig. (3D'). (B') merge of green (infected cells) and magenta (endothelium) fluorescence; (B'') green (infected cells) fluorescence; (B''') magenta (endothelium) fluorescence. White and yellow arrowheads: areas of colocalization.

(C'-C''') SINV infection, fixation at 2 dpi followed by clarity treatment and immunolabeling for GFP and RFP, lateral views; (C') Entire larva, boxes indicate the magnified areas in (C'') and (C'''); (C'') 3D rendering of the heavily infected area encompassing gills, liver, and hindbrain. See **Movie 3**, for rotation of the 3D structure; (C''') High magnification of the infected area in the tail region. White arrowheads: infected cells close to but not part of the vasculature. Scale bars: 150 μ m.

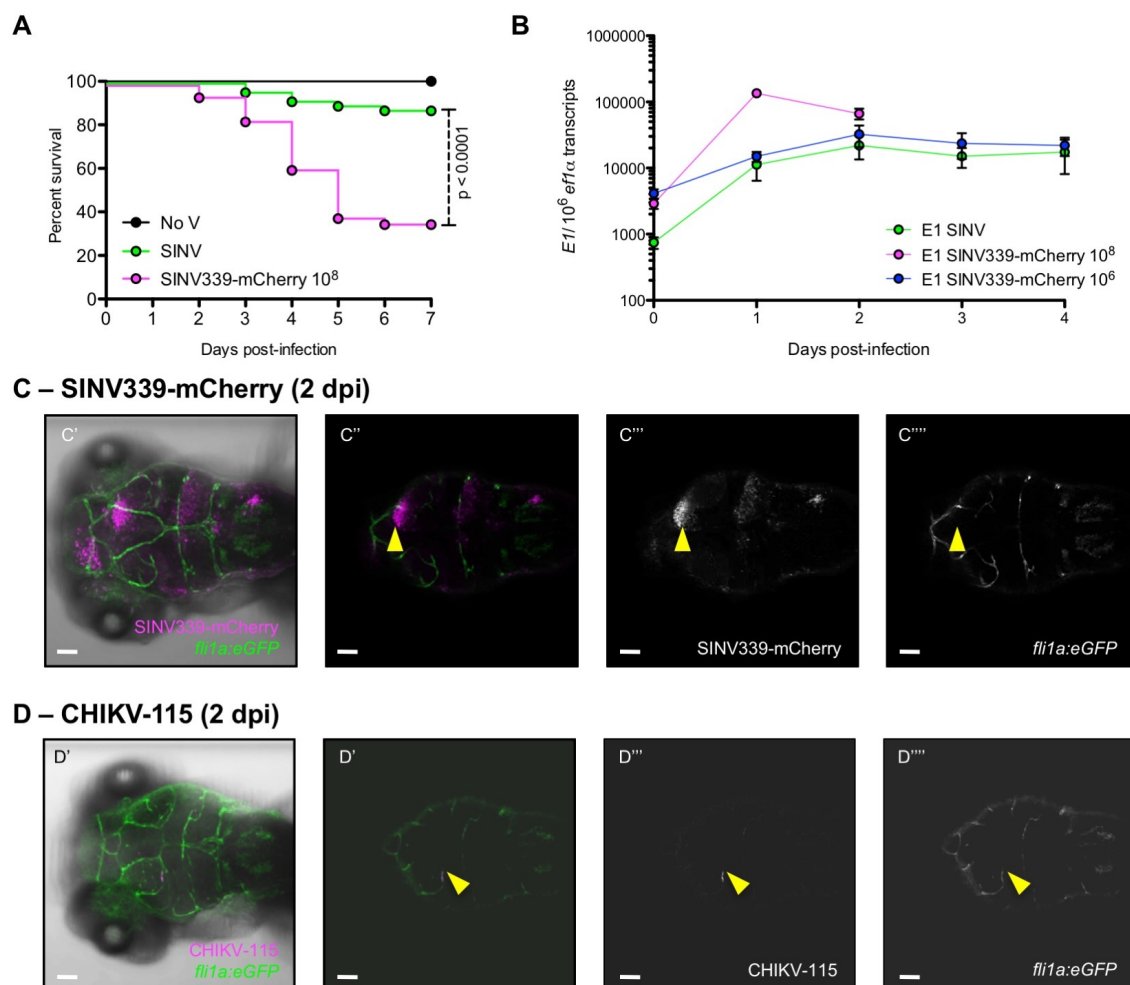


Figure S2. Infection of zebrafish larvae with other SINV and CHIKV strains.

(A and B) Characterization of SINV339-mCherry strain in zebrafish WT larvae. (A) Survival curves of control uninfected (No V) and SINV- or SINV339-mCherry infected zebrafish larvae. Data pooled from 5 independent experiments. N = 60 larvae per group. (B) Expression levels of E1 SINV gene, measured via qRT-PCR, for SINV and SINV339-mCherry (2 different concentrations). Note that at the highest concentration, all SINV339-mCherry infected larvae had succumbed at 2 dpi.

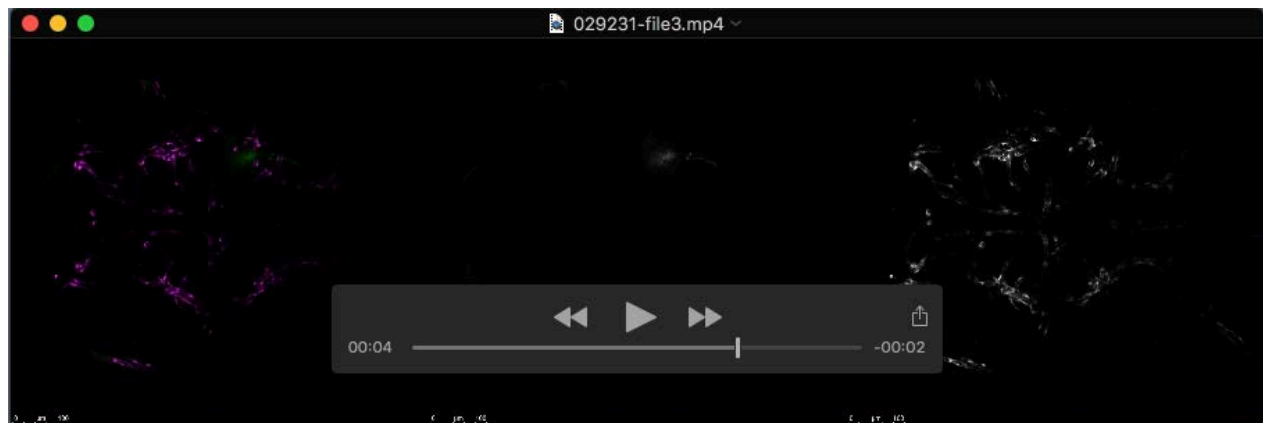
(C and D) Confocal image of WIHC processed SINV339-mCherry (C) and CHIKV-115 (D) infected *fli1a:eGFP* larvae, (C' and D') maximal projection. Scale bars: 50 μ m. (C'-C''') SINV-infected cells in magenta; vasculature in green. (C'') merge of magenta (infected cells) and green (endothelium)

fluorescence from a single focal plane; (C'') magenta (infected cells) fluorescence; (C''') green (endothelium) fluorescence. Yellow arrowheads: infected areas close to but not part of the vasculature. (D'') merge of magenta (infected cells) and green (endothelium) fluorescence from a single focal plane; (B'') magenta (infected cells) fluorescence; (B''') green (endothelium) fluorescence. Yellow arrowheads: areas of colocalization.

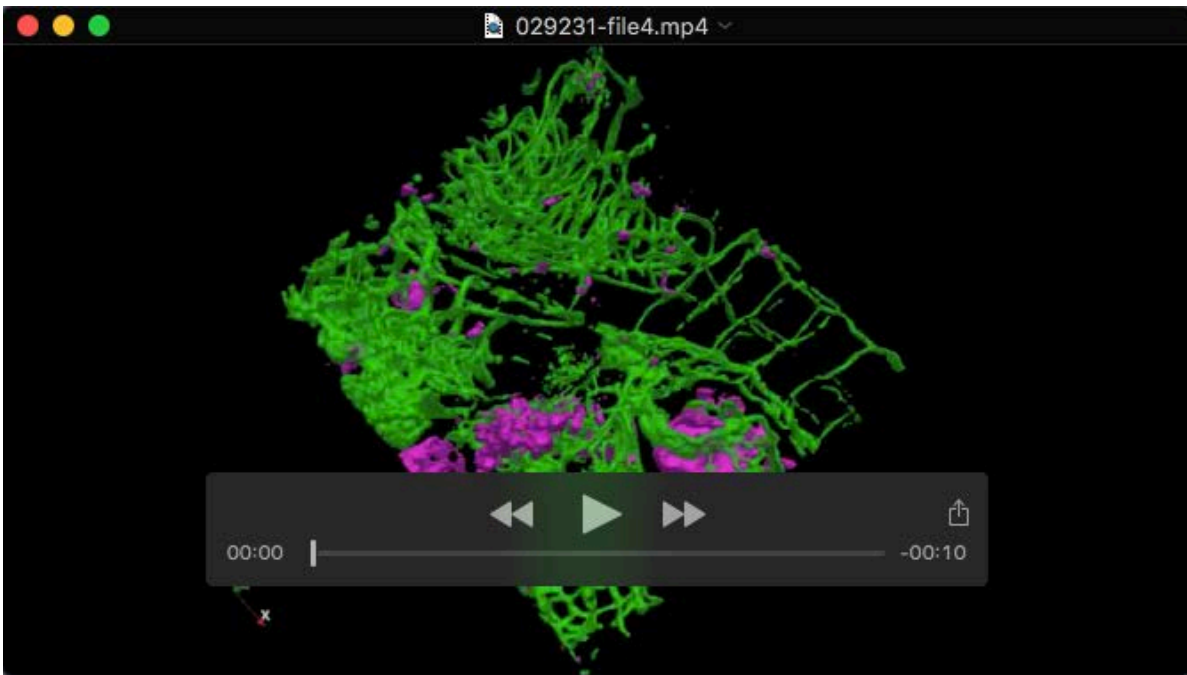
Supplementary movies



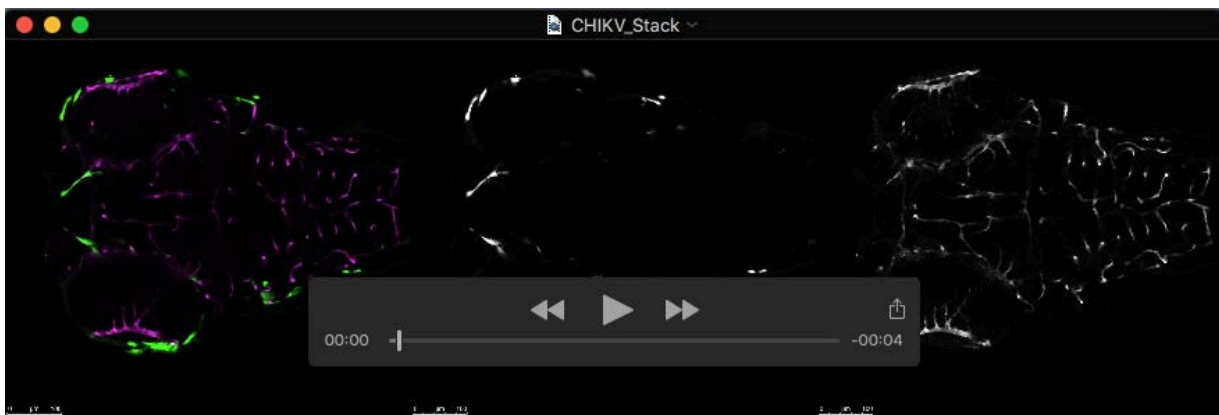
Movie 1. Movement through Z-stacks of *fli:G/U:RFP* SINV-infected larva, at 2 dpi. Related to Fig. 3B.



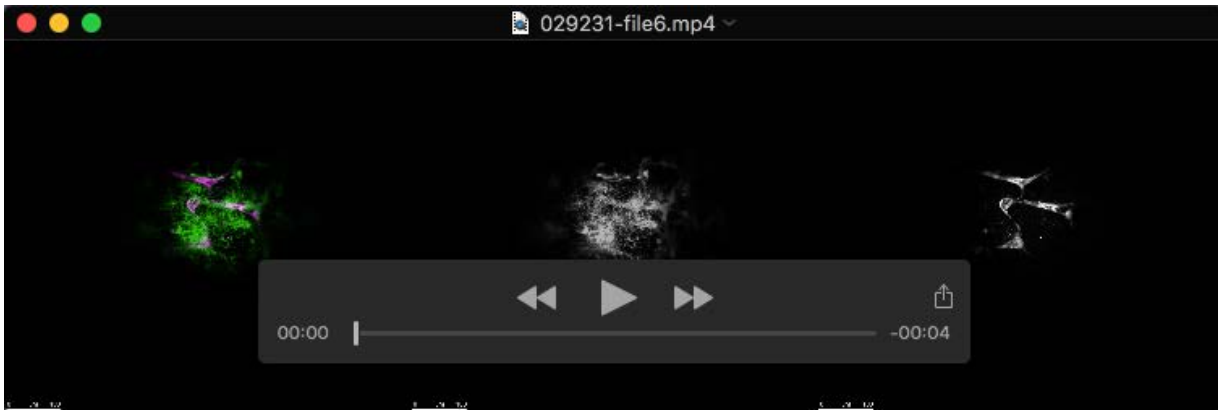
Movie 2. Movement through Z-stacks of the same *fli:G/U:RFP* SINV-infected larva, at 1 dpi. Related to Fig. 3A.



Movie 3. 3D rendering of *fli:G/U:RFP* SINV-infected larva. Related to Fig. S1D.



Movie 4. Movement through Z-stacks of *fli:G/U:RFP* CHIKV-infected larva, at 1 dpi. Related to Fig. 3D.



Movie 5. Movement through Z-stacks of *fli:G/U:RFP* IHNV-infected larva, at 2 dpi. Related to Fig. 3F.